Non-rigid 2D/3D Registration for Patient Specific Bronchoscopy Simulation with Statistical Shape Modelling: Phantom Validation

Fani Deligianni, Adrian J. Chung, Guang-Zhong Yang*

Abstract— **This paper presents a non-rigid 2D/3D registration framework and its phantom validation for subject-specific bronchoscope simulation. The method exploits the recent development of 5 DoF miniaturised catheter tip electromagnetic trackers such that the position and orientation of the bronchoscope can be accurately determined. This allows the effective recovery of unknown camera rotation and airway deformation, which is modelled by an Active Shape Model (ASM). ASM captures the intrinsic variability of the tracheo-bronchial tree during breathing and it is specific to the class of motion it represents. The method reduces the number of parameters that control the deformation, and thus greatly simplifies the optimisation procedure. Subsequently, *pq*-based registration is performed to recover both the camera pose and parameters of the ASM. Detailed assessment of the algorithm is performed on a deformable airway phantom, with the ground truth data being provided by an additional 6DoF EM tracker to monitor the level of simulated respiratory motion.**

Index Terms— **non-rigid 2D/3D Registration, Virtual Endoscope, Virtual Bronchoscopy, Simulation, Respiratory Motion**

I. Introduction

Minimal invasive procedures are playing an increasingly important role in surgery in recent years due to the shortened recovery time, reduced patient trauma, and improved therapeutic outcome. These procedures, however, require a high degree of manual dexterity and hand-eye coordination due to the complexity of instrument control and restricted vision. Effective training is therefore essential for their safe practice in clinical environments.

Conventionally, surgical training is based on the apprenticeship model. Under the scrutiny of experienced instructors, surgical trainees learn by observing, then gradually performing specific procedures inside the operating theatre. The theoretical knowledge of the process is assumed to be gained beforehand through learning. Although the operating theatre is a basic element of surgical training, it is becoming less effective due to several factors. First of all, trainees are exposed to heterogeneous distribution of procedures depending on the flow of patients; it is time consuming and costly. Moreover, operating theatre based training can constitute a potential risk to patients due to the inevitable distraction while training on complex or advanced procedures. This can result in large variations in the professional standards of surgeons. For this reason, a number of laboratory based training approaches have been considered.

With the steady advances of medical imaging and computer graphics techniques, it is now possible to perform patient realistic training based on simulation devices. This considerably decreases the discomfort and risk induced to the patient, as well as the cost involved in the training procedure. It has also the potential to provide a more complete training curriculum by incorporating usual, as well as rare pathological cases combined with objective assessment of surgical skills [1, 2].

Bronchoscopy is a common minimal access diagnostic procedure with which an endoscope is inserted through the nose or mouth into the lungs. The procedure provides a view of the airways and allows the collection lung secretions or tissue biopsy. In practice, bronchoscopy is a difficult procedure to perform and there are significant clinical benefits in using synthetic images for computer-based training simulators. Thus far, a number of experimental and commercial prototype bronchoscope simulators based on abstract or idealized models have been developed [3, 4]. These models are useful for acquiring basic psychomotor skills, particularly the hand-eye coordination and instrument control, but their value for advanced skills assessment is questionable due to the lack of patient-specific perceptual realism [1, 5]. To overcome this problem, the reliance on patient specific data for building anatomical models both in terms of biomechanical fidelity and photorealism has attracted extensive interests in recent years [6, 7]. Existing work has already demonstrated that by fusing real-bronchoscopy video with 3D tomographic data of the same patient, it is possible to generate photorealistic models that allow high fidelity, patient specific bronchoscope simulation [8, 9].

The prerequisite of generating photorealistic models for bronchoscope simulation is accurate 2D/3D registration of 2D bronchoscopy video with 3D tomographic data. Existing 2D/3D registration methods have explored a number of different approaches based on intensity, as well as geometrical features [10, 11]. These methods, however, are generally concerned with the estimation of the pose of the endoscope camera, and the deformation of the intra-thoracic airways is not explicitly modelled. Although being successful for proximal airways, its value for modelling

Funded by the UK Engineering and Physical Sciences Research Council (EPSRC), the Wolfson foundation and the Royal Society.

* Correspondence E-mail: g.z.yang@imperial.ac.uk, Royal Society/ Wolfson Foundation Medical Image Computing Laboratory, Department of Computing, Imperial College London, SW7 2BZ.

distal branches is limited due to the large scale deformation introduced by respiration. In general, the shape of the airway is mainly affected by respiration and cardiac motion. During inspiration, active muscle-driven expansion of the rib-cage and diaphragm leads to expansion of the airways, which draws air into the lungs. The abdominal contents move downward and forward, thus increasing the volume of the thorax [12]. During expiration, the muscles relax and the lung contracts passively via its natural recoil, thus expelling the air. The air can also be actively pushed out of the lungs during respiratory manoeuvre such as forced expiration [13]. During coughing, large airways including the trachea and first several generations of airways tend to collapse dynamically, narrowing to a small fraction of their initial cross-sectional area. Fig. 1 demonstrates the potential challenges involved in free-form 2D/3D registration where structural deformation and artefacts due to bleeding, extreme airway distortion, and occlusion are illustrated. It is important to appreciate that the airways undergo extensive deformation even during normal breathing. Recent developments in CT and MRI have permitted the complete coverage of the lung periphery and airways during different stages of the respiratory motion such that patient-specific deformable models can be constructed [14, 15].

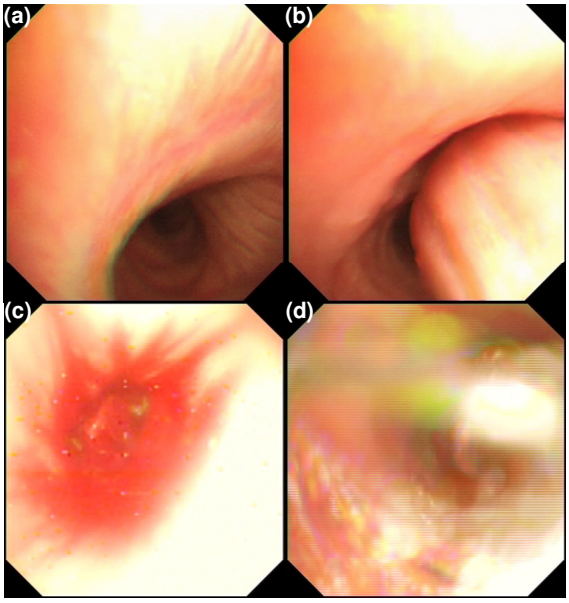

Fig. 1: Examples illustrating the potential challenges involved in free-form 2D/3D registration where structural deformation (a-b), artefacts due to bleeding (c), and occlusion (e) are demonstrated.

The incorporation of airway deformation to the existing 2D/3D registration framework, however, is a difficult task. This is due to the potentially very large degrees of freedom involved in simultaneous tracking of the camera pose and structural changes. The purpose of this paper is to propose a practical 2D/3D registration framework that incorporates patient-specific airway deformation as captured by 3D tomographic imaging and the recent development in catheter tip EM tracking. Currently, the miniaturised EM trackers can be made sufficiently small to be inserted into catheters or biopsy channels of the endoscopes. Under the existing 2D/3D registration framework, they can be used to improve the robustness of the registration techniques as most methods to date require favourable initialisation conditions to ensure a successful registration.

Another important implication of the introduction of the *in vivo* catheter tip EM tracking is that it is now possible to explicitly incorporate airway deformation into the registration framework due to the reduced dimensionality of the search space. At a first glance, it may seem that the use of 5 DoF catheter tip EM tracker reduces the original 2D/3D registration to only a 1D problem. It has been postulated that in the absence of airway deformation, one can readily use the EM tracking result to recover the unknown axial camera rotation [16]. For situations with large, non-linear deformation as encountered in *in vivo* experiments, however, the nature of the problem is much more difficult. This is because the EM tracker reports only the position and orientation of the bronchoscope camera in relation to the fixed, world coordinates. When this information is used to guide the registration of the airway structure reconstructed from the tomographic data, a large displacement due to airway deformation can be observed [17]. When this EM tracking information is used to initialize the 2D/3D registration, it has been found that the initial view can often be completely outside of the bronchial tree. This initialization is in fact inferior to the traditional image based approach, as in this case the camera view is always in synchrony with the moving frame of reference of the deforming airways. For this reason, direct mapping of the EM tracking measurements to the static preoperative CT images is not appropriate, and its practical use must be considered with the deformation of the airways.

Fig. 2 provides a schematic illustration of the proposed registration framework. Given a number of volumetric images at different respiratory phases of the tracheo-bronchial tree, an ASM capturing the intrinsic deformation of the airway is created. Based on the control points of the ASM, Radial Basis Functions (RBFs) are used to warp the 3D mesh to reflect the structural deformation induced. 2D/3D registration is then used to recover both the parameters of the ASM and the pose of the bronchoscope camera. We demonstrate in this paper that by modelling the deformation of the airways with ASM, it is possible to capture intrinsic variabilities of the tracheo-bronchial tree based on images acquired at different phases of the respiratory cycle. In this way, the dimensionality of the non-rigid 2D/3D registration problem can be significantly reduced, thus leading to a rapid and robust registration framework that can be deployed to patient bronchoscope examinations. To our knowledge, this is the first attempt of 2D/3D bronchoscope registration with explicit deformation modelling. This paper provides a comprehensive phantom validation of the proposed registration framework with known ground truth.

II. METHODS

A. Phantom Construction and Data Acquisition

In this study, the airway phantom was made of silicon rubber and painted with acrylics. The inner surface was

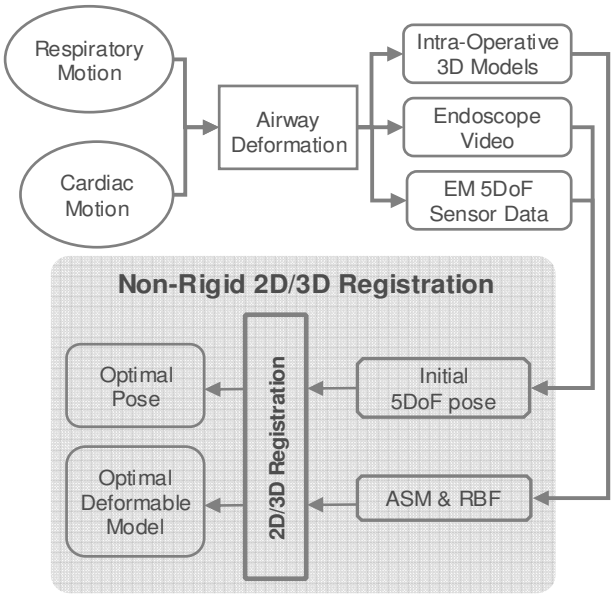

Fig.2: A schematic illustration of the proposed non-rigid 2D/3D registration framework with 5 DoF EM tracking and ASM for deformation modelling.

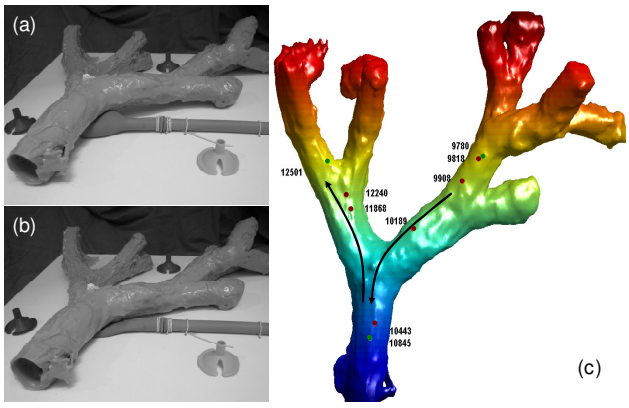

Fig. 3: (a-b) Illustrations of the phantom setup during two different deformation stages and the bronchoscope navigation paths involved in this study (c), where the camera travels from the right branch (frame-9780) to the trachea (frame-10845) and then continues to the left branch (frame-12501).

coated with silicon-rubber mixed with acrylic to give it a textured and specular finish that is similar to the bronchial lumen. The phantom surface was finished with red colour splashes to imitate the blood and texture discrepancies during a bronchoscope examination. The distal ends of the airway-phantom have been fixed and a balloon is located below the main bifurcation to simulate respiratory-induced airway deformation as shown in Fig. 3. In this figure, the navigation paths used for validation are also indicated. The extent of the airway motion is regulated by a valve controlling the amount of air in the balloon. The tomographic model of the phantom was scanned with a Siemens Somaton Volume Zoom 4-channel multi-detector CT scanner with a slice thickness of 1 mm and in-plane resolution of 1 mm. A total of six *CT* volumes were acquired at different stages of the motion cycle.

To track the pose of the bronchoscope camera, an NDI (Northern Digital Inc, Ontario) Aurora EM tracker was used. The Aurora system is particularly suited for tracking flexible endoscopes during minimally invasive intervention. This typically employs a single coil sensor due to size restrictions imposed by the biopsy channel. Having only a single coil, however, the sensor is limited to reporting position and direction only (*i.e.* 5 DoF with unknown axial rotation). The working volume of the Aurora system is within 500mm cube located 50mm from the field generator. In an environment that is free from electromagnetic interference, the Aurora has a static positional accuracy of 0.9-1.7mm and an orientation accuracy of 0.5 degrees [18, 19].

In order to obtain the ground truth deformation data, a real-time, 6 DoF EM tracker tool was used to track the deformation of the balloon so that the deformation of the phantom airway can be indexed back to the 3D CT data. An Olympus bronchoscope (Olympus BF Type, with a field of view 120°) operating in PAL recording mode (25fps) was used to capture the 2D bronchoscope video.

B. Deformation Modelling

For the modelling of airway deformation, the Point Distribution Model (PDM) of the ASM is used such that a compact representation of the deformation of all the control points can be captured by the principal modes of shape variation. In this way, the degree of freedom during deformable 2D/3D registration is only dictated by the number of modes chosen plus the extra degree of freedom introduced by the unknown axial rotation of the endoscope.

ASMs are parametric deformable models that deform in ways that are consistent with the class of shape and motion they represent [20]. This is defined by the boundary point distribution of a number of shapes, called a training set. To ensure that the ASM captures the intrinsic shape rather than the corresponding landmark point variations, all shapes in the training set should be aligned so as to minimise the distance variance of corresponding control points. Subsequently, Principal Component Analysis (PCA) is applied to the PDM to extract the statistical modes of variations that describe these shapes.

The intuitive benefit of ASM derives from the fact that for most deformable models the landmark points are not moving independently, so the intrinsic dimension is significantly lower than the number of control points. Let s_i be a vector describing the n control points of the i^{th} shape of the deformable model

$$s_i = \left(x_{i0}, y_{i0}, z_{i0}, \ldots, x_{ik}, y_{ik}, z_{ik}, \ldots, x_{in-1}, y_{in-1}, z_{in-1}\right)^T \qquad (1)$$

Each sample in the training set can therefore be represented by a single point in a 3*n*-dimensional space. A set of N deformable shapes (6 for this study) results in N points in the 3*n*-dimensional space. These points in general lie within a region of the shape space, which is called the 'allowable shape domain' [20]. Given that every 3*n*-dimensional point within this domain gives a set of landmarks whose shape is similar to those in the original training set, the variability of the shape can be modelled in a systematic way in the remapped space. By assuming that the allowable shape domain is approximately ellipsoidal, its centre can be calculated as the mean shape $\bar{s}$, *i.e.*,

$$\bar{s} = \frac{1}{N}\sum_{i=0}^{N} s_i \quad (2)$$

Subsequently, the principal axes of the ellipsoid fitted to the data are calculated by applying PCA to the data. Each axis gives a mode of variation, which represents the way that the landmark points tend to move together as the shape varies. For each shape in the training set, the deviation from the mean ds_i is calculated to form the covariance matrix S:

$$S = \frac{1}{N}\sum_{i=0}^{N} ds_i ds_i^T \quad \text{with } ds_i = s_i - \bar{s} \quad (3)$$

In this way, any point in the allowable shape domain can be modelled by taking the mean shape and adding a linear combination of the eigenvectors of the covariance matrix, *i.e.*,

$$s = \bar{s} + Pb \quad (4)$$

where $P = (p_1, \ldots, p_t)$ is the matrix of the first t eigenvectors. Therefore, new shapes are generated by varying the parameters b_k within the suitable limits for them to fit to the training set. The limits for b_k are derived by examining the distributions of the parameter values required to generate the training set. In this study, the set of the parameters $\{b_1, \ldots, b_t\}$ is chosen by assuming that the plausible shape variations lie within three standard deviations of the mean.

$$-3\sqrt{\lambda_k} \le b_k \le 3\sqrt{\lambda_k} \quad (5)$$

where λ_k is the k^{th} eigenvalue. This choice covers the plausible shapes between the two extreme shapes at maximum 'exhalation' and 'inhalation' of the phantom.

C. Point Correspondence for the Active Shape Model

As mentioned earlier, in practical implementations the quality of a statistical shape model relies heavily on the accuracy of the landmark correspondence across the 3D model with different levels of structural deformation. In order to establish correspondence between a set of control points across the 3D meshes, the skeleton of the airway was first extracted from the 3D data. The skeleton points were estimated from each slice as the geometric centroid of the surface extracted from the marching cube algorithm. Manual interaction was required to define the bounding box of each branch. The bifurcations of the airway tree were then used as the landmarks for establishing the correspondence across the skeletons. For each of the skeleton points, the surface perpendicular to the skeleton axis was subsequently defined and its intersection with the 3D mesh was estimated. For simplicity, four surface control points corresponding to each skeleton landmark were used. This in general is sufficient to define a branching generalised cylinder for the airways.

D. Mesh Warping using Radial Basis Functions

The application of ASM to the skeletal and surface control points results in intermediate, deformed airway structures. To generate a smooth 3D mesh of the airways, Radial Basis Functions (RBFs) are used [21, 22]. An RBF is a continuous function, of at least C^1 continuity that provides smooth, controllable deformation. It maps each control point in one domain to the corresponding control point in the other with interpolation of the mapping at intermediate points. An RBF spatial transformation in d dimensions, denoted $T(x,y)$, is composed of $k = 1, \ldots, d$ mapping functions [21], such that:

$$T(\vec{x}) = \left[f_1(\vec{x}), \ldots, f_k(\vec{x}), \ldots, f_d(\vec{x})\right] \quad (6)$$

With RBFs, each of the mapping functions can be decomposed into a global component and a local component, and this decomposition enables a family of transformations to be defined where the influence of each control point can be determined. Given n pairs of corresponding control points, each of the k mapping functions of the RBF takes the following form:

$$f_k(\vec{x}) = P_{mk}(\vec{x}) + \sum_{i=1}^{n} A_{ik} g(r_i) \quad (7)$$

where $\vec{x} = (x, y, z)$, $P_{mk}(\vec{x})$, is a polynomial of degree m, $g(r_i)$ is a radial basis function, r_i denotes the Euclidean norm defined by

$$r_i = \left\|\vec{x} - \vec{x}_i\right\| \quad (8)$$

and A_i corresponds to the i^{th}-column of the parameter array W. It is worth noting that the polynomial term has been omitted and $g(r_i)$ is a linear radial basis function that expresses the contribution of each control point on the original vertex.

In the 3D case represented in this study and ignoring the polynomial term of (7), the RBF transformation is determined by n coefficients in each dimension. The coefficients of the function $f_k(\vec{x})$ are determined by constraining $f_k(\vec{x})$ to satisfy the interpolation conditions and solving the following linear system of equations:

$$W = G^{-1}Y \quad (9)$$

where $G(i,j) = g(r_{ij})$, and Y is a matrix with the deformed points. Intuitively, $g(r_{ij})$ measures the effect of the j^{th} control point on the transformation at the i^{th} control point. The above equation is typically solved by using Singular Value Decomposition (SVD) and the new position of each vertex is then calculated from (7). During calculation, since the vertices have been changed the normals also need to be recalculated. In this study, the normals for each rendered scene are implicitly estimated as part of the registration procedure [23].

E. 2D Video Preprocessing

Prior to 2D/3D registration, pre-processing of the videos was necessary in order to alleviate the effects of interlacing, lens distortion, and image artefact [23]. De-interlacing can

be achieved by separating odd/even scan lines, which is particularly important to minimise the comb effect during fast advancement or retraction of the bronchoscope. To correct for barrel distortion due to the wide angle bronchoscope camera used, the camera model suggested by Heikkila [24], which includes both radial and tangential distortion of the video image, was used. The initialization of the calibration parameters follows the work by Zhang et al [25]. Finally, to improve the SNR of the video image, a structure adaptive anisotropic filter was used [26]. The method uses a local orientation and anisotropic measure to control the shape and extent of the filter kernel and thus ensures that salient image features are well preserved whilst removing image artefacts. The method generally provides a smoother optimisation landscape, and brings improved convergence of the 2D/3D registration algorithm.

F. Deformable 2D/3D Registration

The deformable registration framework used in this study consists of four main components as shown in Fig. 2. These include the ASM that represents the non-rigid deformation of the mesh based on a reduced set of parameters, the RBFs that control the deformation to the mesh, the EM tracking data used to initialise the camera pose, and finally the optimisation phase where both the camera pose and mesh deformation parameters are determined. The EM tracker provides 5 DoF out of 6 DoF that are needed to fully describe the motion of the endoscopic camera. They first need to be transformed into the 3D mesh coordinate system. For this reason, three landmarks have been added to the phantom such that by touching them with the tip of the EM tracker, a rigid transformation between the two coordinate systems can be determined based on a close-form solution [27, 28].

The basic principle of constructing a similarity measure for the 2D/3D registration is based on the original *pq*-based framework proposed by the authors [23, 29]. In this technique, surface normals of the video endoscopic image are extracted by using a linear shape from shading algorithm, which exploits the unique endoscopic camera/lighting special configuration. During registration, these vectors are matched to the surface normals of the 3D model with its deformation controlled by the ASM and axial camera rotation. The similarity measure of the two images was determined by evaluating the dot product φ of the corresponding *pq*-vectors. By incorporating the mean angular differences and the associated standard deviations σ, the following similarity function is used:

$$S = \left\{ \sum \sum (\varphi_w) \cdot \sum \sum \left(\left\| 1 - \sigma(\varphi_w) \right\| \cdot \left\| \bar{n}_{3D} \right\| \right) \right\}^{-1} \qquad (10)$$

where $\bar{n}_{3D}$ is the surface normals derived from the 3D model and φ_w stands for the weighted dot product. With this scheme, neither the lighting parameters nor the other rendering parameters need to be adjusted during registration. The similarity measure is weighted according to the 3D model surface vectors, such that it is relatively immune to texture discrepancies that are common to the endoscopic images. For optimising the above similarity measure, the Simplex algorithm by Nelder and Mead was used [30].

G. Validation

In this study, the ground truth data used was provided by the 6-DoF EM tracker attached to the balloon controlling the level of simulated respiratory motion. This permits the direct association of the deformation of the airway phantom during bronchoscope examination with the exact 3D geometrical shape captured by CT. The projections of the deformation as mapped onto the principal axes defined by the ASM were used in this study to provide a quantitative measure of the effectiveness of the registration process, i.e.,

$$b_1 = \vec{M} \cdot p_r \cdot \left(p_r \cdot p_r^T \right)^{-1} \qquad (11)$$

where p_r is the eigenvector that corresponds to the point s_r of the 3D mesh that is nearest to the position of the 6-DoF EM tracker, and $\vec{M}$ is the vector between these two points.

III. RESULTS

To demonstrate the general visual appearance of the phantom airway model, Fig. 4 illustrates 9 example frames of the video sequence after pre-processing, which includes de-interlacing, lens distortion correction, and anisotropic smoothing. The result of applying the ASM to the reconstructed 3D volumes are also shown in Fig. 4, illustrating the warped 3D mesh by using the RBF along the first principal mode of the shape variation in the sagittal, coronal and axial views. The red, green, and blue meshes correspond to varying $-3\sqrt{\lambda}_1$, 0, and $+3\sqrt{\lambda}_1$ from the mean shape, which are the extreme values of the allowable shape domain. Table 1 shows the total modelling error associated with each eigenvalue. The coefficients of all six eigenvectors are estimated by minimising the mean squares error between the target control points and the shape defined by the ASM. Subsequently, the error due to the omission of each eigenvector is calculated. It is evident that the first principal component captures most of the airway deformation, which means that even by varying the first mode alone, most of the structural deformation as reconstructed by RBF can be used to control the subsequent 2D/3D registration process.

To demonstrate the amount of deformation introduced, the normalised mesh displacement map at four different deformation positions of the phantom are shown in Fig. 5, illustrating the non-linear, localised deformation at different branches of the airway. By reference to the navigation paths shown in Fig. 3, it is evident that we have chosen the most deformed part of the airway phantom for the validation purpose.

For the results presented in this paper, a conventional PC with an AMD Athlon™, 2.19GHz, 1GB RAM and a graphic card NVIDIA GeForce 6800 Ultra was used. The rendering was based on OpenGL and the graphical interface is designed using FLTK (Fast Light ToolKit). The airway mesh consisted of 13,101 vertices and 26,101 triangles. The code has not been optimised and each frame took around 3 minutes to optimise.

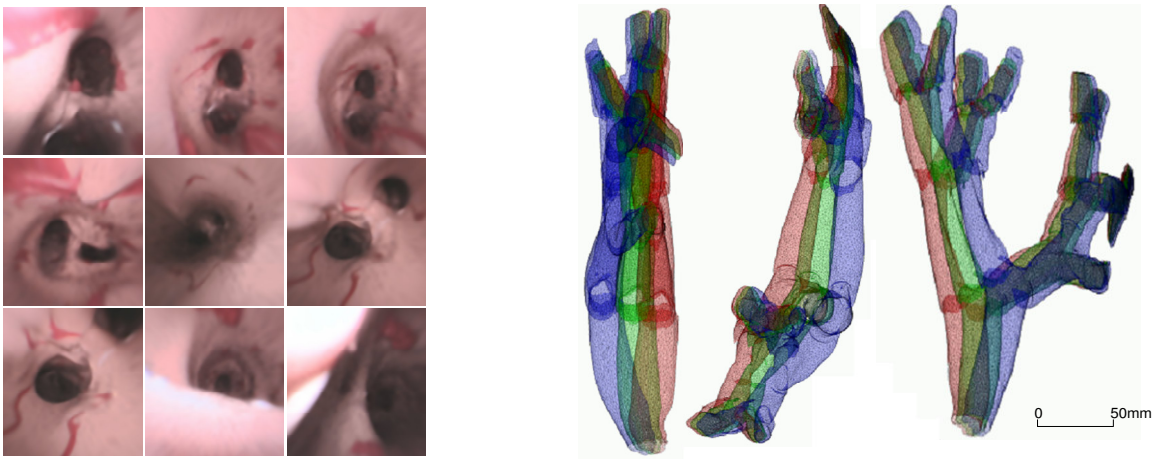

Fig. 4: Left - Example bronchoscope video frames acquired during the phantom experiment where the images have been pre-processed to alleviate the effect of interlacing and lens distortion. Right - The result of applying the ASM to the reconstructed 3D volumes, illustrating the warped 3D mesh by using the RBF along the first principal mode of the shape variation. The red, green, and blue meshes correspond to varying $-3\sqrt{\lambda}_1$, 0, and $+3\sqrt{\lambda}_1$ from the mean shape.

For the ASM, 301 control points have been used and the RBF has been implemented such that the initialisation step is calculated only once to estimate the inverse of G matrix of (10), which represents the topology of the initial control points. The rest part of the calculation was almost completely dedicated to the deformation of the vertices based on (7).

The performance of the proposed registration algorithm by using the EM tracking data combined with the deformable model as determined by ASM can be examined in Fig. 6. In this figure, the top row is the bronchoscope view of the phantom airway, whereas the middle row illustrates the corresponding view of the 3D model determined by the 5 DoF catheter tip EM tracker. Significant mis-registration is evident due to the unknown rotation and airway deformation. The result of applying the proposed registration algorithm is shown in the bottom row of Fig. 6, demonstrating the visual accuracy of the method.

In order to provide a detailed quantitative validation of the method, Fig. 7 illustrates the recovered deformation as projected onto the first principal axis of the ASM model. In other words, this reflects how parameter b_1 controls the shape of the mesh based on (4). The corresponding ground truth value as determined by the 6 DoF EM tracker from (11) is also provided for comparison. It is evident that the reconstruction result followed the ground truth reasonably well. Further details of the error analysis are illustrated in Fig. 8, which provides a Bland-Altman plot of the errors of the recovered deformation as compared to the ground truth.

IV. Discussion and Conclusions

In this paper, we have proposed a deformable 2D/3D registration framework based on ASM. Despite the prevalence of tissue deformation in most surgical navigation and planning applications, its incorporation into the 2D/3D registration framework has been limited. This is due to the large degrees of freedom involved in the registration parameters, which make a stable implementation of the algorithm difficult.

The recent advance of miniaturised catheter tip EM trackers has greatly simplified the 2D/3D registration process. For rigid registration, existing 5 DoF EM tracker inserted to the biopsy channel of the endoscope can provide much improved results as the remaining 1 DoF is relatively easy to optimise. For deformable airways, however, existing research has shown that complex deformation of the anatomical structure still represents a major problem to the registration process despite the use of the catheter tip EM tracker [16]. In this case, direct application of local deformation to the 3D structural mesh to match to that of the bronchoscope video is computationally impractical due to the large number of control points involved. Furthermore, issues such as mesh folding also need to be carefully addressed. Although it is possible to use the finite element model to provide bio-mechanically plausible model to define airway deformation, its practical implementation can be difficult due to the general lack of detailed tissue mechanical property, as well as the prohibitive computational cost involved.

In this study, we have demonstrated that the use of ASM provides a simple yet effective framework for a compact representation of the airway deformation. This allows deformation to be modelled by the limited principal modes of variation such that conventional optimisation processes can be effectively applied. Statistical shape models and PDMs in particular, provide an effective means of capturing statistically plausible variations of the shape of the object. The ASM combines a model-based approach similar to template models that allow for large variability with *a prior* knowledge incorporated through a number of previous observations. It has a number of advantages for its use in a non-rigid 2D/3D registration framework. The method describes both typical shape and intrinsic deformation and the motion variability is accommodated through prior knowledge incorporated through the 3D data. Therefore, they can effectively model the deformation of the structure even though the motion mechanisms are not sufficiently understood, or too complex to derive. Furthermore, they are specific to the class of motion they represent, and hence can be implemented in a subject specific manner.

It should be noted, however, that the effectiveness of the method depends on the ability of the 3D models in capturing possible structural deformations during video bronchoscope

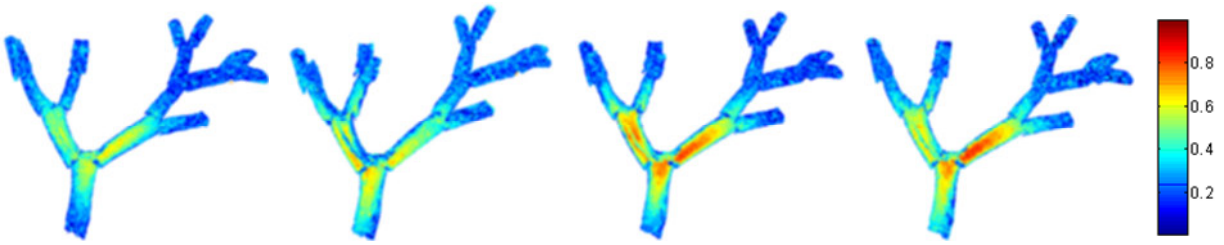

Fig 5. The normalised mesh displacement between successive deformation stages of the phantom.

TABLE 1. MODELLING ERROR ASSOCIATED WITH OMITTING EACH EIGENVALUE INDIVIDUALLY.

EigenValues in Descending order	1st	2nd	3rd	4th	5th	6th
Error in mm	4.3542	0.7723	0.6170	0.1482	0.055	0.0
Error in percentage (%) of the phantom diameter	10.88	1.93	1.54	0.3706	0.1392	0.0

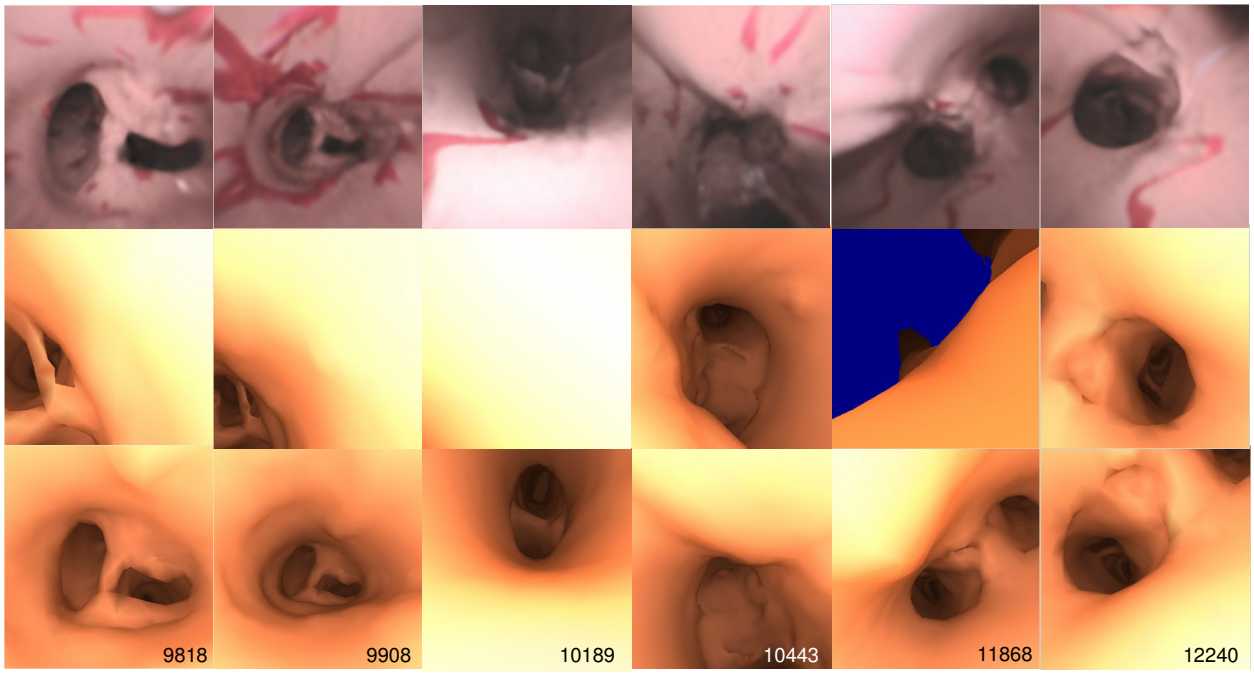

Fig. 6: The performance of the proposed registration algorithm by using the EM tracking data combined with the deformable model as determined by ASM. Top-row: the bronchoscope view of the phantom airway; Mid-row: the corresponding view of the 3D model determined by the 5 DoF catheter tip EM tracker where significant mis-registration is evident due to unknown rotation and airway deformation; Bottom-row: the result of applying the proposed registration algorithm demonstrating the visual accuracy of the method.

examination.

For the phantom experiment presented in this paper, we have used CT to provide the structural information of the airways.

This, however, may not be suitable for patient studies as the capture of airway deformation at different phases of the respiratory cycle for constructing the ASM model can involve significant ionising radiation. A more practical choice would be to use the recent developments of MRI that permits the visualisation of the lung parenchyma and airways during normal physiological motion [14, 15]. The combination of respiratory navigator echoes will allow the imaging of the intra-thoracic tree at different stages of the respiratory motion, and therefore the construction of a complete deformable model of the airways on a subject-specific basis.

It is also important to note that with the proposed registration framework, the global motion of the patient must be monitored during bronchoscope examination such that it is removed from the catheter-tip EM tracking data for localising the catheter tip in relation to the CT scan volume. This is an issue not encountered in the traditional image registration framework as global motion of the patient will result in a synchronous movement of the bronchoscope and

the airways. This problem, however, can be addressed by tracking externally the position and orientation of the patient during bronchoscope examination [17, 31]. The advantage of the proposed method is that it provides a practical way of handling airway deformation. In addition, EM tracking allows the continuation of the registration process when extreme breathing patterns and artefacts caused by mucosa, bubbles, bleeding are encountered. In a typical examination, these effects account for 20-30% of the procedure and they

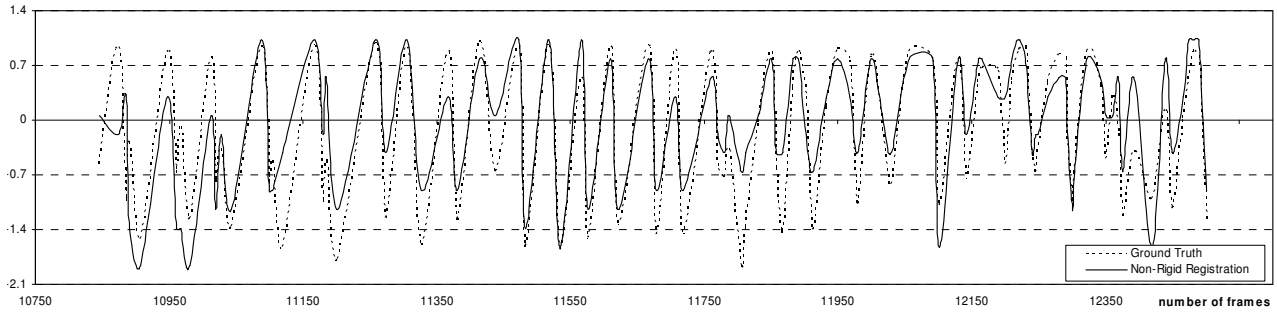

Fig 7. The recovered deformation as projected onto the first principal axis of the ASM model where the corresponding ground truth value (dotted curve) as determined by the 6 DoF EM tracker from Equation (11) is provided for comparison.

can reach almost 100% in extreme cases, such as profuse haemoptysis.

These effects interleave during common bronchoscope procedures, thus providing only short video sequences where image-based registration approaches are successful. When the registration fails it is not trivial to recover the camera position and re-initialise the algorithm. EM tracking, however, is much more immune to these problems [17]. The use of 5 DoF catheter tip EM tracker combined ASM can provide a closer approximation of the camera pose such that the exact solution to the problem can be limited to a localised search space. Patient data also indicates that at the bifurcation/turning points, a rigid model is relatively difficult to smoothly follow the video frames, since the pre-operative and intra-operative 3D structures may not be in correspondence.

In terms of localised airway deformation, one additional problem that deserves consideration is that in typical tomographic imaging the patient is positioned in a supine position, whereas in bronchoscope examinations the patient typically adopts an upright posture. It is feasible that the deformation of the intra-thoracic airways due to the gravity effect may be different due to the variation in pose. This, however, is a problem that is encountered by all 2D/3D registration techniques.

It should also be noted, that the success of ASM depends on the number and quality of correspondent landmarks across the observable shapes. In this paper, we used a simplistic method to extract the skeleton of the tracheo-bronchial tree and subsequently correspondence was established based on the matching of the bifurcation points. The identification of optimal control points for ASM for complex topological shapes, however, is a significant challenge [32].

Since the ASM is based on landmark correspondence, effective way of smoothly interpolating the mesh points with regard to the motion of the control points is necessary. In this paper, we used RBF for a number of reasons. Firstly, the distribution of the control points can be both sparse and irregular. RBF provides an easily controllable behaviour that can be tailored to meet specific requirements. It may be purely deformable, or contain some forms of linear component to allow for both localised and global deformations [21]. Other techniques such as (NURBS) [12] based surface representation is also possible for creating the dynamic model of the airway. The actual computational complexity for estimating each new vertex with RBFs is $O(nN)$, where *n* is the number of control points and N is the number of vertices. The solution of the equation system in the pre-processing step requires an additional . Here we calculate the SVD only at the initialisation stage of the algorithm since the topology of the points does not change. Therefore, the time required depends mainly on the number of vertices of the 3D model, which are usually much larger than the number of control points. These time requirements can also be optimised. For example, the mesh can be deformed only locally since the bronchoscope only provides a localised view of the airways. Other improvements such as to bind locally the radial basis functions and use parallel processing can also be introduced [21].

In this study, the main purpose of the phantom design is to assess the extent of free-form deformation and its effect on the accuracy of 2D/3D registration. It should be noted that the phantom is not a complete representation of the airway structure and its physiological response. The air flow patterns and the force distribution on the airway conduits are patient-specific and they vary significantly across different subjects [33]. Since the ASM model is to be constructed on a patient-specific basis, the proposed phantom validation framework should provide a good indication of the achievable accuracy of the algorithm for in vivo applications.

In conclusion, we have developed a non-rigid 2D/3D registration framework that models the respiratory motion of the intra-thoracic tree which incorporates the EM tracking data for improved robustness and accuracy. ASM has been used to capture the intrinsic variability of the airways across different phases of the respiratory motion and it also constrains the motion they represent to be specific to the subject studied. This allows the subsequent non-rigid registration implemented in a much reduced dimensional space, and thus greatly simplifies the 2D/3D registration procedure. The detailed phantom validation of the method in this study demonstrates the potential clinical value of the technique.

V. Acknowledgements

The authors would like to acknowledge the financial support of the EPSRC, the Royal Society and the Wolfson Foundation. They are also grateful to Professor David M. Hansell and the radiographer Nina Acuri (MD) for scanning the phantom and providing the CT data.

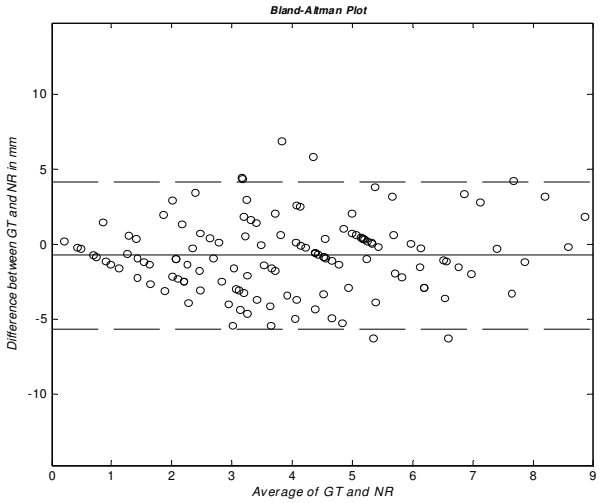

Fig. 8: Bland-Altman plot of the non-rigid registration results as compared to the ground truth.

VI. REFERENCES

[1] R. M. Satava, "Surgical Education and Surgical Simulation," *World Journal of Surgery*, vol. 25, pp. 1484 - 1489, 2001.

[2] A. Liu, F. Tendick, K. Cleary, and C. Kaufmann, "A Survey of Surgical Simulation: Applications, Technology, and Education," *Presence*, vol. 12, 2003.

[3] H. G. Colt, S. W. Crawford, and O. Galbraith, "Virtual Reality Bronchoscopy Simulation: A Revolution in Procedural Training," *Chest*, vol. 120, pp. 1333-1339, 2001.

[4] M. Bro-Nielsen, "Simulation Techniques for Minimally Invasive Surgery," *Journal of Minimally Invasive Therapy & Allied Technologies (MITAT)*, vol. 6, pp. 106-110, 1997.

[5] R. S. Haluck, R. L. Marshall, T. M. Krummel, and M. G. Melkonian, "Are Surgery Training Programs Ready for Virtual Reality? A Survey of Program Directors in General Surgery.," *Journal of American College of Surgeons*, vol. 193, pp. 660-665, 2001.

[6] A. Chung, F. Deligianni, M. Elhelw, P. Shah, A. Wells, and G. Z. Yang, "Assessing Realism of Virtual Bronchoscopy Images Via Specialist Survey and Eye-Tracking," presented at Medical Image Perception Conference XI (MIPS XI), Abstract, Windermere, UK, 2005.

[7] J. P. Helferty and W. E. Higgins, "Combined Endoscopic Video Tracking and Virtual 3D CT Registration for Surgical Guidance," presented at International Conference on Image Processing, IEEE 2002 (ICIP'00), Rochester, New York, 2002.

[8] M. A. ElHelw, B. P. Lo, A. J. Chung, A. Darzi, and G. Z. Yang, "Photorealistic Rendering of Large Tissue Deformation for Surgical Simulation," presented at International Conference on Medical Image Computing and Computer Assisted Intervention (MICCAI04), Saint-Malo, France, 2004.

[9] M. A. ElHelw, S. Atkins, M. Nicolaou, A. Chung, and G. Z. Yang, "Photo-Realistic Tissue Reflectance Modelling for Minimally Invasive Surgical Simulation," presented at International Conference on Medical Image Computing and Computer Assisted Intervention (MICCAI05), Palm Springs, California, USA, 2005.

[10] K. Mori, D. Deguchi, J. Sugiyama, Y. Suenaga, J.-i. Toriwaki, C. R. M. Jr., H. Takabatake, and H. Natori, "Tracking of a Bronchoscope Using Epipolar Geometry Analysis and Intensity-Based Image Registration of Real and Virtual Endoscopic Images," *Medical Image Analysis*, vol. 6, pp. 181-336, 2002.

[11] I. Bricault, G. Ferretti, and P. Cinquin, "Registration of Real and CT-Derived Virtual Bronchoscopic Images to Assist Transbronchial Biopsy," *IEEE Transactions on Medical Imaging*, vol. 17, pp. 703-714, 1998.

[12] J. M. Garrity, W. P. Segars, S. B. Knisley, and B. M. W. Tsui, "Development of a Dynamic Model for the Lung Lobes and Airway Tree in the NCAT Phantom," *IEEE Transactions on Nuclear Science*, vol. 50, pp. 378-383, 2003.

[13] O. E. Jensen, "Flows through Deformable Airways," 2002.

[14] A. C. Tooker, K. S. Hong, E. L. McKinstry, P. Costello, F. A. Jolesz, and M. S. Albert, "Distal Airways in Humans: Dynamic Hyperpolarized (3)He MR Imaging—Feasibility," *Radiology*, vol. 227, pp. 575-579, 2003.

[15] T. A. Sundaram, B. B. Avants, and J. C. Gee, "A Dynamic Model of Average Lung Deformation Using Capacity-Based Reparameterization and Shape Averaging of Lung MR Images," presented at (MICCAI2004), Rennes, Saint-Malo, France, 2004.

[16] K. Mori, D. Deguchi, K. Akiyama, T. Kitasaka, C. R. Maurer, Y. Suenaga, H. Takabatake, M. Mori, and H. Natori, "Hybrid Bronchoscope Tracking Using a Magnetic Tracking Sensor and Image Registration," presented at International Conference on Medical Image Computing and Computer Assisted Intervention (MICCAI05), Palm Springs, California, USA, 2005.

[17] S. B. Solomon, P. J. White, C. M. Wiener, J. B. Orens, and K. P. Wang, "Three-Dimensional CT-Guided Bronchoscopy with a Real-Time Electromagnetic Position Sensor: A Comparison of Two Image Registration Methods," *Chest*, vol. 118, pp. 1783-1787, 2000.

[18] D. D. Frantz, A. D. Wiles, S. E. Leis, and S. R. Kirsch, "Accuracy Assessment Protocols for Electromagnetic Tracking Systems," *Phyisics in Medicine and Biology*, vol. 48, pp. 2241-2251, 2003.

[19] G. Corral, K. Cleary, J. Tang, E. Levy, and N. Glossop, "Orientation Accuracy of a Magnetic Tracking Device for Image-Guided Interventions," presented at Computer Assisted Radiology and Surgery (CARS), 2002.

[20] T. F. Cootes, C. J. Taylor, D. H. Cooper, and J. Graham, "Active Shape Models: Their Training and Application," *Computer Vision and Image Understanding*, vol. 61, pp. 38-59, 1995.

[21] D. Ruprecht and H. Muller, "Image Warping with Scattered Data Interpolation," *IEEE Computer Graphics and Applications*, vol. 15, pp. 37-43, 1995.

[22] M. A. Wirth, D. Nikitenko, and J. Lyon, "Matching 3D MR Breast Images Using a Localized Radial Basis Function," presented at International Society for Magnetic Resonance in Medicine, Toronto, Canada, 2003.

[23] F. Deligianni, A. Chung, and G. Z. Yang, "Patient-Specific Bronchoscope Simulation with pq-Space-Based 2D/3D Registration," *Computer Aided Surgery*, vol. 9, pp. 215-226, 2004.

[24] J. Heikkila and O. Silven, "A Four-Step Camera Calibration Procedure with Implicit Image Correction," presented at IEEE Computer Society Conference on Computer Vision and Pattern Recognition (CVPR97), San Juan, Puerto Rico, 1997.

[25] C. Zhang, J. P. Helferty, G. McLennan, and W. E. Higgins, "Nonlinear Distortion Correction in Endoscopic Video Images," presented at International Conference on Image Processing, 2000, Vancouver, BC Canada, 2000.

[26] G. Z. Yang, P. Burger, D. N. Firmin, and S. R. Underwood, "Structure Adaptive Anisotropic Image Filtering," *Image and Vision Computing*, vol. 14, pp. 135-145, 1994.

[27] B. K. P. Horn, "Closed-Form Solution of Absolute Orientation Using Unit Quaternions," *Optical Society of America A*, vol. 4, pp. 629-642, 1987.

[28] A. J. Chung, P. J. Edwards, F. Deligianni, and G. Z. Yang, "Freehand Cocalibration of an Optical and Electromagnetic Tracker for Navigated Bronchoscopy," presented at The Second International Workshop on Medical Imaging and Augmented Reality (MIAR 2004), Beijing, China, 2004.

[29] F. Deligianni, A. Chung, and G. Z. Yang, "pq-Space 2D/3D Registration for Endoscope Tracking," presented at Medical Image Computing and Computer Assisted Intervention (MICCAI03), Montréal, Québec, Canada, 2003.

[30] J. A. Nelder and R. Mead, "A Simplex Method for Function Minimization," *Computer Journal*, vol. 7, pp. 308-315, 1965.

[31] F. Deligianni, A. Chung, and G. Z. Yang, "Decoupling of Respiratory Motion with Wavelet and Principal Component Analysis," presented at Medical Image Understanding and Analysis (MIUA04), London, UK, 2004.

[32] P. Horkaew and G. Z. Yang, "Optimal Deformable Surface Models for 3D Medical Image Analysis," presented at Information Processing in Medical Imaging (IPMI), 2003.

[33] J. R. Cebral and R. M. Summers, "Tracheal and Central Bronchial Aerodynamics Using Virtual Bronchoscopy and Computational Fluid Dynamics," *IEEE Transactions on Medical Imaging*, vol. 23, pp. 1021-1033, 2004.